OPEN ACCESS

University of BRISTOL

Bowen, L., Celik, A., Azarpeyvand, M., & Il\'{a}rio da Silva, C. R. (2021). *Porous geometry effects on the generation of turbulence interaction noise*. Paper presented at AIAA Aviation Forum 2021, United States. https://doi.org/10.2514/6.2021-2193

Peer reviewed version

Link to published version (if available):
10.2514/6.2021-2193

Link to publication record in Explore Bristol Research
PDF-document

This is the author accepted manuscript (AAM). The final published version (version of record) is available online via American Institute of Aeronautics and Astronautics at 10.2514/6.2021-2193. Please refer to any applicable terms of use of the publisher.

University of Bristol - Explore Bristol Research
General rights

This document is made available in accordance with publisher policies. Please cite only the published version using the reference above. Full terms of use are available:
http://www.bristol.ac.uk/red/research-policy/pure/user-guides/ebr-terms/

Porous geometry effects on the generation of turbulence interaction noise

Luke Bowen*, Alper Celik†, Mahdi Azarpeyvand‡
Faculty of Engineering, University of Bristol, BS8 1TR, UK

Carlos R. Ilário da Silva§
Embraer, Sáo José dos Campos, 12227-901, Brazil

Turbulence interaction noise between a turbulent inflow and an airfoil with various porous leading edges has been experimentally investigated. The effect of multiple parameters of the porous structure at the leading edge of a NACA 0012 airfoil on the aeroacoustic characteristics were investigated at a chord-based Reynolds number of 2.6×10^5. The airfoil was additive manufactured and has an interchangeable leading edge allowing for porous structure to occupy up to 20% of the chord. The turbulent inflow was generated by placing a grid within the contraction nozzle which does not affect the normal background noise of the wind tunnel jet. The effect of the porous leading edges were quantified by direct noise measurement and was compared to the results of a solid leading edge. It is found that far-field noise was reduced for low frequency in most cases, but incorporation of the porous material introduces a penalty of high frequency noise. An increase in the porous-occupied volume at the leading edge increases the level of surface pressure fluctuation at low frequency, and increases the level of coherence in both spanwise and streamwise direction.

I. Introduction

In the drive towards a more sustainable future, noise pollution is becoming a predominant environmental concern. One form of flow that can contribute to noise pollution is turbulent flow. When a turbulent flow comes into contact with a body immersed in the flow it generates noise, which in the right conditions can be a efficient generator of noise. Turbulent flow can be generated by the rotating motion of a fan, which is generally highly rotational. To increase the efficiency of a rotating fan, the flow is straighten downstream of the fan. The impinging turbulence on the flow straighteners causes fluctuating pressure forces on the surface of the body which generates noise. This is mechanism of interest, turbulence interaction noise. To understand the fundamental problem of turbulence interaction noise this configuration can be simplified to an airfoil immersed into a turbulent flow. The nature of this interaction noise is such that the geometry of impingement is an important factor, as is the qualities of turbulence impingement itself. Variations in the turbulent structure sizes cause different qualities of interaction noise. Turbulent structures cause pressure fluctuations at the leading edge of the airfoil which generate noise. When these structures are large comparatively to the geometry they are impinging on, this noise generation mechanism can become very efficient. To understand the effect of changing the leading edge structure with the same geometry, the turbulent structures must be larger than the leading edge radius.

Turbulence interaction noise is a subject that has been of large social interest for some time and historically has been well studied. Paterson and Amiet [1] originally proposed the idea of turbulence impingement as low frequency dominating noise radiation, considering the scale of turbulence is large. Amiet went on to propose a model [2] which can predict the interaction noise by first using linearized theory to calculate the aerodynamic response of the incident gust on the airfoil; then calculating the unsteady lift propagation to the acoustic far-field accounting for scattering and mean flow effects. Moreau and Rodger [3] studied the effects that angle of attack has on noise generation in turbulent flow and showed there is almost no dependency angle of attack. Devenport et al. studied the effects of real airfoils in turbulence [4] and concluded that although angle of attack has a strong effect on the airfoil response function, it only has a small effect on noise generation. Celik et al. [5] demonstrated that the low sensitivity of the surface pressure response to the angle of attack extends to the energy spectra of lift and drag too. As turbulent inflow conditions are an

*Ph.D Student, Department of Mechanical Engineering, luke.bowen@bristol.ac.uk
†Postdoctoral Research Associate, Department of Mechanical Engineering, alper.celik@bristol.ac.uk
‡Professor of Aerodynamics and Aeroacoustics, Department of Mechanical Engineering, m.azarpeyvand@bristol.ac.uk
§Challenge Owner in Electrifying Aviation, Embraer, Sáo José dos Campos, Brazil, carlos.ilario@embraer.com.br

important factor, this was extensively studied by Hutcheson et al. [6] consisting of a host of different inflow conditions and geometries, finding that as length scale and intensity increased this uniformly increased the spectral levels. As the geometry is an important factor in the noise generation there have been many studies subject to this [3, 4, 7–9], all finding that the airfoil geometry does in fact alter the noise generation in turbulent flow.

Active [10, 11] and passive [12–18] noise control techniques have shown in many instances that they are effective methods of noise reduction when well implemented into trailing edges. Turbulence interaction noise has previously shown that it can be reduced by using passive leading edge treatments, and the use of serrations has had an increasing level of interest in recent years [18–23]. Interaction noise reduction with porous materials has also been the subject of many previous studies and shows a viable method for a correctly implemented solution to the reduction of noise generated at the leading edge. Rodger et al. [24, 25] used grid generated turbulence to measure the effect that a steel-wool filled NACA 0012 had on noise radiation and showed a maximum of 5dB of noise reduction is achievable from a sub-optimal approach. Geyer and Sarradj have carried out multiple studies on porous airfoils [26–28], the first study on the effect of fully porous airfoils in turbulent flow [26]. The study focused on changing porous properties of airfoils to assess the acoustic benefit, a reduction in noise for most cases was found at the detriment to the overall hydrodynamic performance of the airfoil. Further works have showed the potential of porous materials for noise reduction [12, 29–34], but a common conclusion is found that better understanding of the mechanisms and flow interaction is needed to optimise the implementation of porous materials for the noise abatement. Zamponi et al. [35] conducted boundary layer measurements around a porous airfoil to better understand the flow conditions. As with previous studies [12, 13] they found that the porous material will decrease the low frequency noise contribution and increase at high frequency, suggested to be surface roughness [13].

This study investigates the effect of changing the porous geometry at the leading edge on the turbulence interaction noise. A matrix of leading edge porous geometry is explored and compared to a solid baseline to understand how changing the chordwise amount of the leading edge that is porous-occupied can affect the noise generated by a NACA 0012 airfoil. A grid is used to generate the turbulent flow in an anecohic wind tunnel without affecting the normal background noise of the wind tunnel jet. The study considers the aerodynamic analysis of the implementation of the porous leading edges, the effect the porous leading edge has on the far field noise as well as the near field noise, measured by microphones at the surface of the airfoil.

II. Measurement setup

A. Wind tunnel and model

The experiments were performed in the University of Bristol Aeroacoustic Facility, which is a closed-circuit, open-jet anechoic wind tunnel. Figure 1 displays a schematics of the wind tunnel contraction with turbulence grid, the airfoil, and a closed-up look of the grid with definitions of the parameters. The chamber has physical dimensions of 6.7 m x 4.0 m x 3.3 m and is anechoic down to 160Hz [36], see Fig. 2. The contraction nozzle outlet has physical dimensions of 500mm in width and 775mm in height which allows for a steady operation from 5 m/s to 45 m/s and a normal turbulence intensity level below 0.2% [36]. The airfoil was a NACA 0012 profile which had a span of 600mm and chord of 200mm. It was manufactured in one piece using the additive manufacturing technique of Selective Laser Sintering (SLS) from polymide. It was designed to be highly instrumented for the measurement of both aerodynamic and aeroacoustic phenomena in the form of static pressure and unsteady surface pressure. This was achieved by the use of brass tubes which were installed with 2 part epoxy resin and smoothed to the surface of the airfoil. In total there were 48 static pressure taps and 88 unsteady surface pressure taps which were drilled with a 0.4mm bit to avoid pressure attenunation at high frequencies. The surface pressure taps were connected in a remote sensing configuration using Panasonic WM-61A microphones [37]. All microphones were calibrated in both magnitude and phase referenced to a single GRAS 40PL microphone, which was calibrated using a GRAS 42AA pistonphone calibrator. Static pressure measurements were obtained from two Chell MicroDaq-32 pressure acquisition systems and were sampled for 32 seconds at 1000Hz.

B. Far field measurement

The turbulence interaction noise was measured using the far field microphone array. The array consists of 23 microphones arranged at 5° increments between polar angles of 35° and 150° to allow for directivity measurements. The arc was located 1.75 m above the airfoil and microphone at 90° was located directly above the leading edge of the

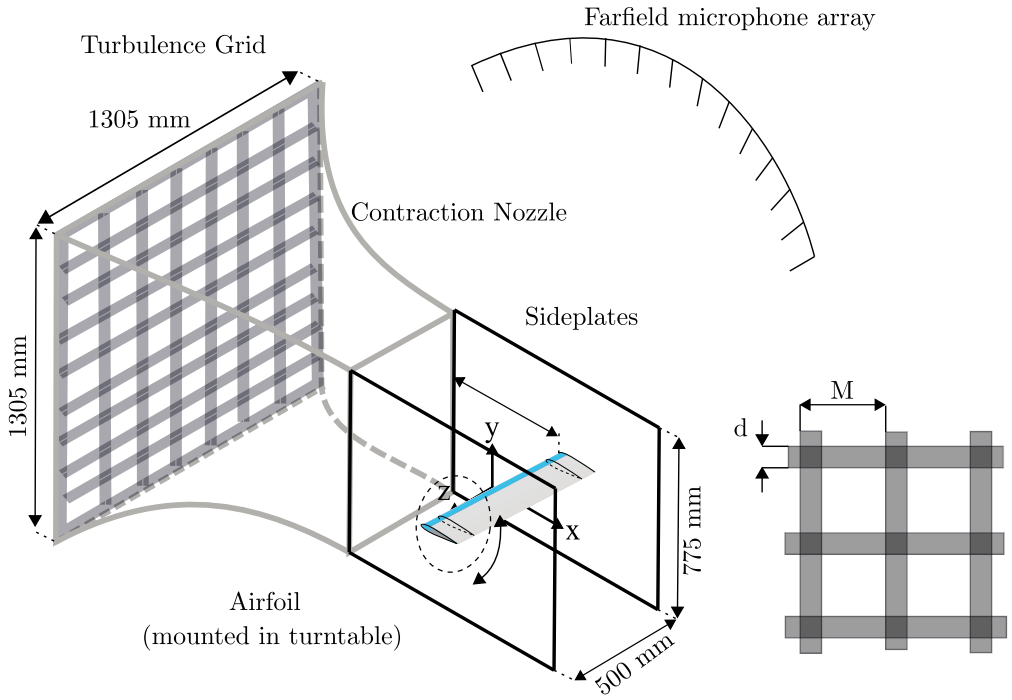

Fig. 1 Schematic of the turbulence-airfoil interaction set up in the aeroacoustic wind tunnel facility at the University of Bristol, including: a grid generating a turbulent inflow, a NACA 0012 airfoil with interchangeable leading edge mounted in side plates, the far field microphone array, and the details of the grid.

airfoil. The microphones on the arc were 1/4 inch GRAS 40PL microphones, which exhibit a flat frequency response for a large dynamic range of 10Hz and 20, 000Hz. All microphones were calibrated using a GRAS 42AA pistonphone calibrator prior to the experiments.

Table 1 The geometric properties of the grid, and the flow properties at the position of contraction nozzle exit, $x = 0$, at a freestream velocity $U_\infty = 20m/s$.

Grid	Diameter, d (mm)	Mesh, M (mm)	σ	Turbulence intensity (%)	Integral length scale (mm)
$C-4$	45	233	0.35	10.1	10.8

C. Turbulence grids

To generate the incoming turbulence, a grid was placed within the contraction nozzle of the wind tunnel. The position of the grid within the tunnel was shown to not affect the normal background jet noise of the wind tunnel [38], thus allowing for direct noise measurement of the interaction noise between the turbulent flow and NACA 0012 airfoil with various porous leading edges. The geometric properties and generated flow properties of the grid are outlined in Table 1.

D. Porous leading edges

Figure 3 illustrates a schematic of the airfoil. The first 20% of the leading edge was interchangeable, between a solid, instrumented leading edge and 3D printed porous structures. A single porous structure was tested constant porosity and permeability in order to understand the effect of increasing the porous-occupied volume at the leading edge of the airfoil in an effort to find an optimum solution for noise reduction. All of the tested leading edged were printed in-house at the

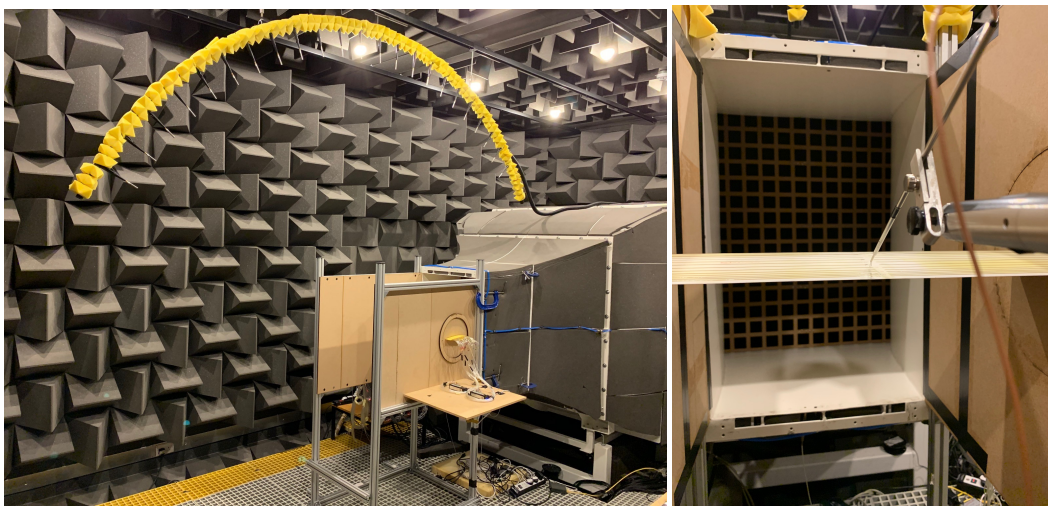

(a) **(b)**

Fig. 2 Picture of the experimental set up within aeroacoustic wind tunnel at University of Bristol, (a) displays the rig, nozzle and far field microphone array, (b) displays the airfoil, and boundary layer CTA hotwire probe and the turbulence grid inside the contraction nozzle.

University of Bristol using a FormLabs Form3 stereolithography (SLA) printer. The tested structure was characterised prior to tests for both porosity and permeability. The porosity was calculated from the generated CAD file as the ratio between the total area and the void area,

$$\varphi = V_V / V_T, \tag{1}$$

where V_V is the volume of the void and V_T is the total volume of the sample. By measuring the pressure drop across the sample, and using the Dupuit-Forchheimer equation the permeability of the sample can be determined. These were measured using a static airflow permeability rig which is displayed in Fig. 4. The measured pressure drop Δp is used in the equation

$$\Delta p / t = \mu / \kappa \upsilon_D + \rho C \upsilon_D^2, \tag{2}$$

where κ is the permeability coefficient, t is this thickness of the sample, ρ is the density of the fluid, C is the inertial loss term and υ_D is the Darcian Velocity which is defined as the volume flow rate divided by the cross-sectional area of the sample. The value of permeability for the structure that is used in this test is $4.4x10^{-9}$ and the structures associated porosity is 50%.

1. Base structures

The mathematically designed surface is displayed in Fig. 5 and is the Schwarz-P surface. This is a Triply-Periodic Minimal Surfaces (TPMS) and was first described by Schwarz [39, 40]. This geometry was selected for the leading edge structure due to its homogeneity in three-dimensions. It was a mathematically designed surfaces which allows for the ease of control over the cell length and the porosity, which ultimately varies the permeability. This base structure is used in all four of the leading edges that were tested. The surface was generated from the control an of the equation where the Schwarz-P surface is defined by

$$\cos(lx) + \cos(ly) + \cos(lz) = a, \tag{3}$$

where l was used to define the unit length, and a was a constant that controls the porosity.

The schematics of the tested leading edges are demonstrated by Fig. 6. In order to study the trends with greater ease, the standard structure was chosen as the Schwarz-P surface, with a porosity of 50% and a cell length of 3mm. The variation was then conducted around this base. The percentage of the leading edge that should be occupied by the porous material was studied by varying between 5% and 20%, in 5% increments, of the leading edge.

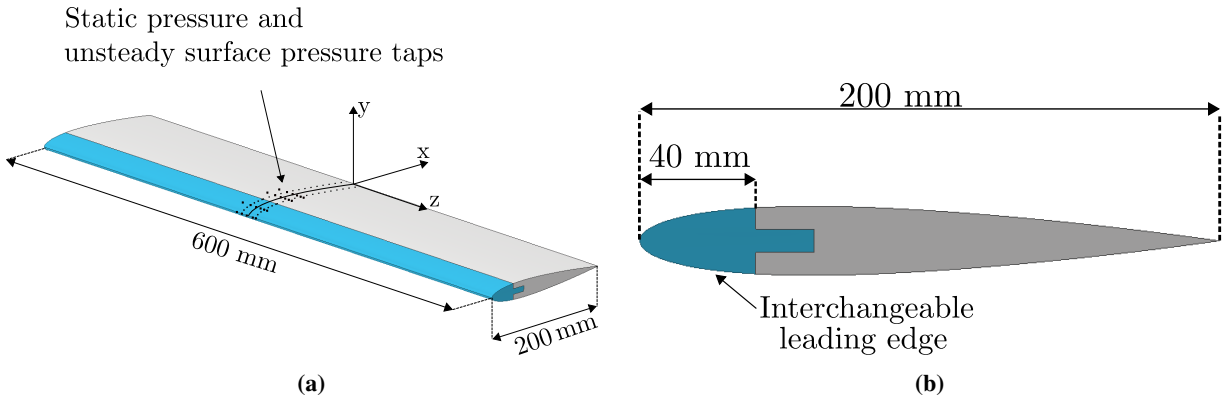

Fig. 3 Schematic of the NACA 0012 airfoil with a 20% x/c interchangeable leading edge, a) Isometric view showing pressure tap and unsteady surface pressure tap locations and b) side view of the airfoil showing the interchangeable part.

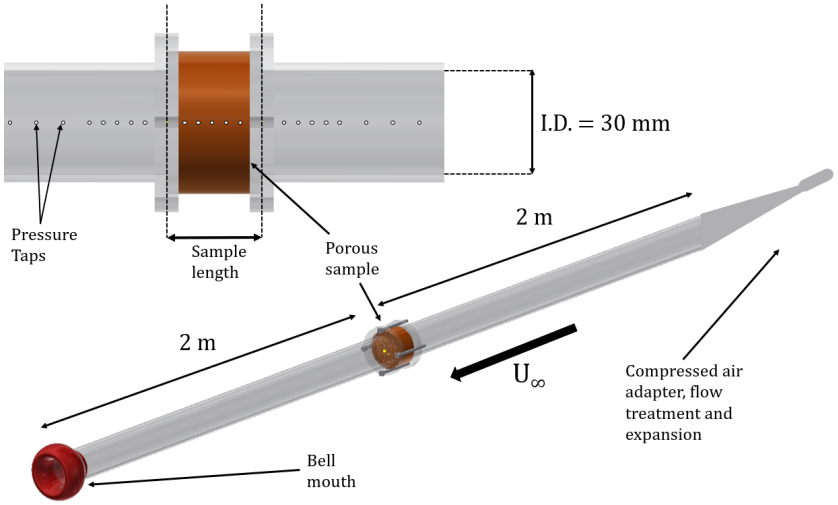

Fig. 4 Permeability rig used to quantify the static airfoil permeability of the porous samples.

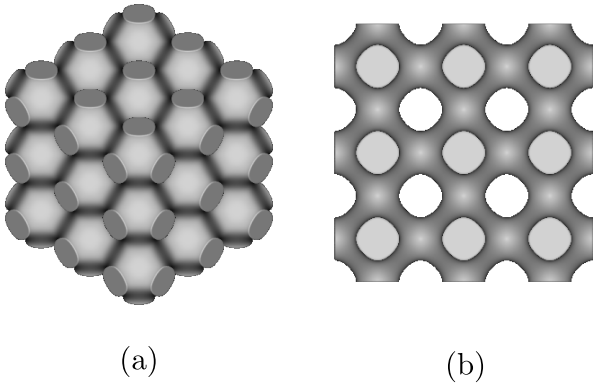

Fig. 5 3x3 cell of triply periodic minimal surface base features used in the generation of porous leading edges where (a) is an isometric view of the Schwarz-Primitive structure and (b) is left view of the Schwarz-Primitive structure.

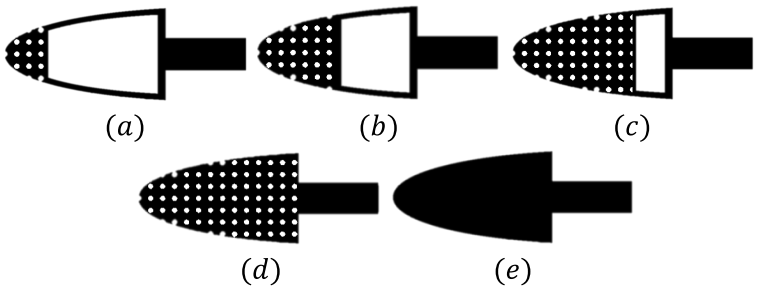

Fig. 6 Schematic of porous leading edge geometries, where: (a) P1, Schwarz-P 5% **of chord, located** $0 < x/c < 0.05$**,** $L = 3$**mm, (b) P2, Schwarz-P** 10% **of chord, located** $0 < x/c < 0.1$**,** $L = 3$**mm, (c) P3, Schwarz-P** 15% **of chord, located** $0 < x/c < 0.15$**,** $L = 3$**mm, (d) P4, Schwarz-P** 20% **of chord, located** $0 < x/c < 0.2$**,** $L = 3$**mm, (e) solid baseline airfoil leading edge.**

III. Results and Discussion

Each of the tested porous leading edges is compared to the solid case in the following section. The leading edges are grouped into each figure and presented with the solid case in order to ease the understanding of the effect the porous leading edge on the turbulence interaction noise. This section first considers the aerodynamic analysis, followed by the far field noise, and lastly the near field analysis.

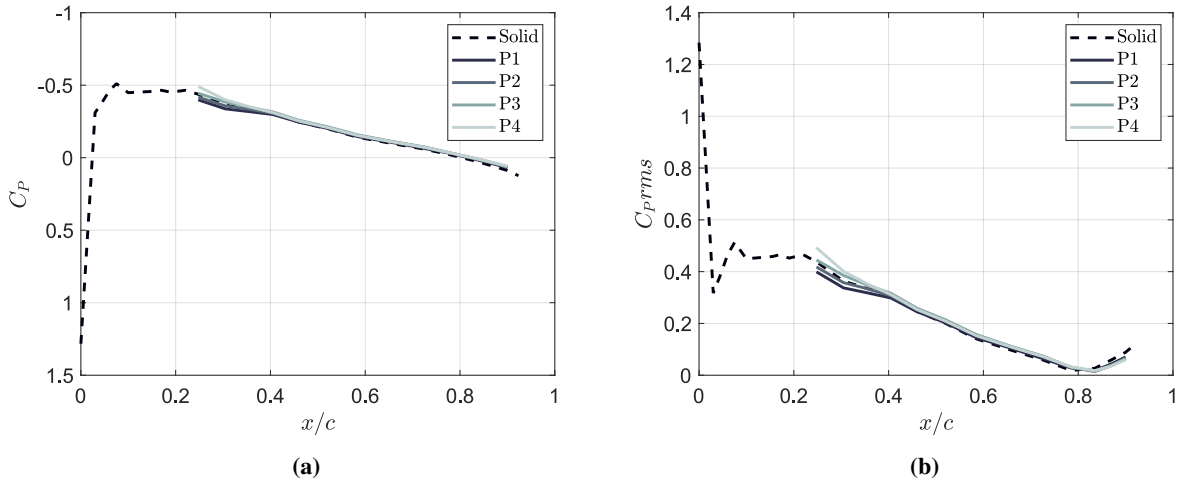

(a) **(b)**

Fig. 7 Schematic of the NACA 0012 airfoil with a 20% x/c **interchangeable leading edge, a) Isometric view showing pressure tap and unsteady surface pressure tap locations and b) side view of the airfoil showing the interchangeable part.**

A. Aerodynamic analysis

This section presents the non-dimensional pressure coefficient measured over the chord of the airfoil, and the root-mean-square (rms) of the pressure coefficient value. As there is no instrumentation over the leading edge of the airfoil, it is not possible to understand the effect of the porous material on the suction peak that is typical of the pressure coefficient distribution over an airfoil. However, the measurement of pressure coefficient immediately downstream of the porous material is considered to understand if there is a further downstream effect caused by the porous leading edge. Figure 7a shows the results of the static pressure in terms of the non-dimensionalized pressure coefficient, C_P, for the NACA0012 airfoil at an angle of attack of $\alpha = 0°$ for a freestream velocity of $U_\infty = 20$ m/s. The results of the C_P distribution are presented as the average value of both solid and suction side of the airfoil for the solid case, and for the four porous cases, P1, P2, P3 and P4. The C_P distribution for the cases with porous inserts is displayed for $0.2 < x/c < 1$, due to a lack of static pressure ports for the porous inserts. The C_P for the solid case shows a distribution

which is expected for a symmetric airfoil and was validated against xFoil in the same manner as Bowen *et. al* [41]. Comparing the C_P distribution of the porous cases to the solid case, the results show that the main area of interest is $0.2 < x/c < 0.3$. The C_P values for cases P1 and P2, show a reduction over the solid case for $0.2 < x/c < 0.3$, where the C_P values for cases P3 and P4 show an increase over the solid case. This could be an indication of the effect of the porous material on the flow field, as the C_P distribution exhibits an increase for cases P1 to P4 over the region $0.2 < x/c < 0.3$. However more information on the local velocity profile is required to elaborate the effect of the porous material on the flow field. Figure 7b shows the results of the root-mean-square of the C_P value for the solid case and the four porous cases P1, P2, P3 and P4. The general trend is an increase for the value of C_{Prms} for P3 and P4 and a reduction for cases P1 and P2, comparable to trend observed in the C_P distribution.

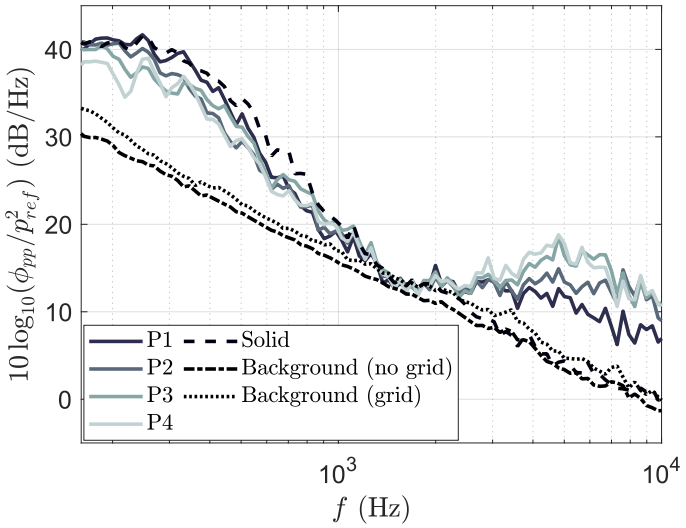

Fig. 8 Power spectral density level of the far field noise obtained by the microphone 90° above the leading edge of the NACA 0012 airfoil with the solid leading edge, and porous cases P1, P2, P3 and P4 at $U_\infty = 20$ m/s.

B. Far field noise

This subsection presents the direct far field noise observation which is generated by the NACA0012 airfoil with various porous leading edges in a turbulent in flow generated by a turbulence grid. The section considers the power spectral density level of the far field noise observed at a polar angle of $\theta = 90^\circ$ over the frequencies 160 Hz$< f < 10,000$ Hz. It is calculated using $PSD = 10 \cdot \log_{10}(\phi_{pp}/p^2_{ref})$, where ϕ_{pp} is the power spectral density of the measured acoustic pressure and p_{ref} is the reference pressure of 20 μPa. Secondly, the overall sound pressure level is presented and the directivity of the radiated noise is considered. The overall sound pressure level is calculated as,

$$OASPL = 10 \cdot \log_{10}\left[\frac{\int \phi_{pp}(f)df}{p^2_{ref}}\right], \tag{4}$$

integrating the energy spectrum with respect to frequency, between 160 Hz$< f < 20,000$ Hz.

Figure 8 shows the leading edge noise spectra for the NACA0012 airfoil at $\alpha = 0^\circ$ for the porous cases P1, P2, P3 and P4 in comparison with the solid leading edge. From the data presented in Fig. 8 the PSD level of the porous cases exhibit a reduction at low frequency and an increase at high frequency, where the crossover is between 1000 Hz$< f <$ 2000 Hz. Compared to the solid case, in general the porous leading edges show a reduction in the PSD level below $f <$ 1000 Hz and above $f >$ 2000 Hz an increase is evident. Recall from Fig. 6 that from P1 to P4 the amount of chord which is porous increases from 5% to 20%. What stands out in this figure is the trend linking the noise reduction to the amount of chord which is porous. When comparing to the solid case, the results of P1 shows the least reduction at low frequency and the results of P4 demonstrate the greatest reduction. At high frequency a similar trend is observed, where the PSD level of P1 generates the least noise increase over the solid case and PSD level of P4 generates the highest

noise increase at high frequency. The most significant level of reduction in the PSD level is generated by leading edge P4, which demonstrates a consistent reduction of up to 4 dB for frequencies 160 Hz$< f <$ 600 Hz. However, the results of P4 also demonstrate an increase of up to 10 dB above a frequency of $f >$ 5000 Hz. To compare the overall acoustic performance of the porous leading edges to the solid leading edge the overall sound pressure level should be examined. This should help quantify the porous leading edges low frequency noise reduction and the high frequency noise increase.

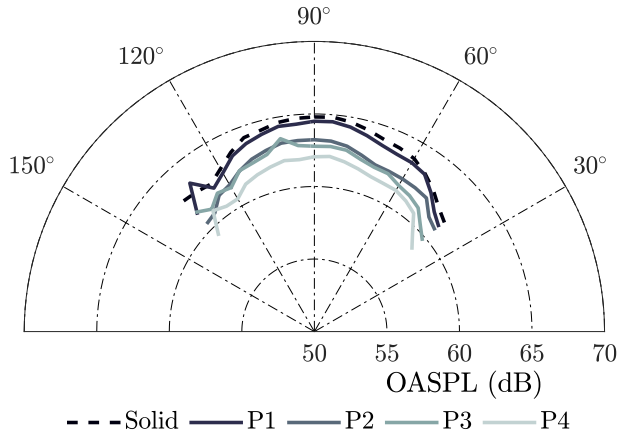

Fig. 9 Directivity of the Overall sound pressure level (OASPL) of the noise generated by the interaction between the turbulent in-flow and the NACA 0012 airfoil with the solid baseline and porous leading edges P1, P2, P3 and P4 at $U_\infty = 20$ m/s.

The overall sound pressure level is employed to understand how the noise generated by the airfoil is directed to the far-field, and how the directivity is affected by the porous leading edges. Overall sound pressure level is obtained by integrating the energy spectrum with respect to frequency. The integration is carried out over the frequency range of 160 Hz$< f <$ 10,000 Hz. Figure 9 shows the directivity of the overall sound pressure level for the solid case and four porous leading edge cases, namely P1, P2, P3 and P4, at angle of attack $\alpha = 0°$ and a freestream velocity of $U_\infty = 20$ m/s. The figure assists in highlighting the trend observed in Fig. 8, the increasing porous-occupied chord resulting in a more significant noise reduction at low frequency. The P4 leading edge causes the greatest reduction in the overall sound pressure level compared the OASPL of the solid case, despite the increase of high frequency broadband noise. Overall, the results of P2 and P3 have very similar OASPL directivity patterns for angles $60° < \theta < 120°$, suggesting that their difference between 10% and 15% of chord being porous-occupied is minimal in terms of the radiated noise. P1 offers the least reduction in OASPL compared to the solid case although it is still a noticeable reduction. Finally, there is no major change to the directivity pattern in all cases compared to the solid case.

C. Near field analysis

The near field analysis is considered in following section. As with the pressure coefficient results, it is not possible to compare the porous section of the airfoil with the solid airfoil due to lack of instrumentation over the porous structure on the leading edge. However, it is possible to compare the immediate downstream effects, and the remainder of the solid part of the airfoil to the trailing edge. This is considered in this section, as the power spectral density of the surface pressure fluctuation and multiple locations over the solid part of the airfoil. This section also considers the spanwise and streamwise coherence of the surface pressure fluctuation. The PSD of the unsteady surface pressure fluctuations for three microphones on the surface of the airfoil, namely $x/c = 0.23$, $x/c = 0.55$ and $x/c = 0.92$, at an angle of attack of $\alpha = 0°$, for all leading edges are shown in Fig. 10. Microphone 10 is the first microphone on the main body of the airfoil following the porous with a corresponding location of $x/c = 0.23$, see Fig. 10a. For the porous leading edge cases this is the first possible measurement location in the streamwise direction from the stagnation point i.e. $x/c = 0$. In each figure the dashed line represents the solid baseline case. Recall that for cases P1 through to P4 there is

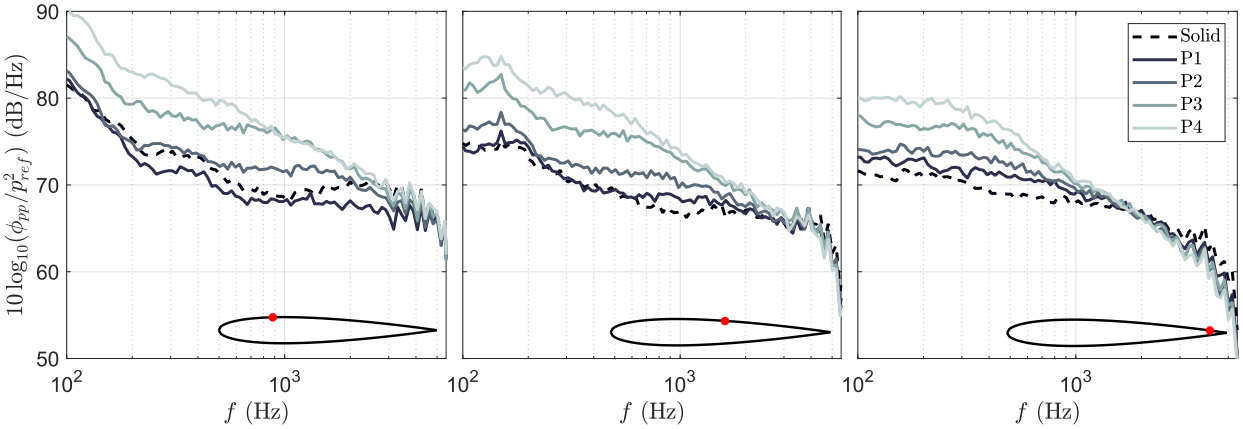

Fig. 10 Power spectral density level of the near-field fluctuations measured by three microphones on the main body of the airfoil at locations $x/c = 0.23$, $x/c = 0.55$ and $x/c = 0.92$, for the solid baseline compared to the porous leading edges at $U_\infty = 20$ m/s.

a chordwise increase in the amount of volume that the porous material occupies, from 5% to 20% respectively. As shown in Fig. 10a the full energy spectra measured by microphone 10 increases from P1 through to P4 up to f=3000 Hz, where the PSD curves converge. The PSD level of P2 shows a comparable trend to the solid case, whereas the energy spectra level for cases P3 and P4 demonstrate an increase for frequencies 100 Hz$< f <$ 3000 Hz on the solid baseline. What is interesting in Fig. 10a is the reduction of the energy spectra level for a leading edge with the first 5% of the chord occupied by the porous structure (P1), compared to the solid case. PSD of the surface pressure fluctuations for microphone 14, which is located further downstream from the porous medium at $x/c = 0.55$, for each leading edge are shown in Fig. 10b. Although the overall energy level reduces, the spatial change from microphone 10 ($x/c = 0.23$) to microphone 14 ($x/c = 0.55$) does not change the overall trend between the PSD results for cases P1, P2, P3 and P4 to the solid case. The results suggest that the effect of the porous material is still evident further downstream of the leading edge. Figure 10c shows the PSD of the unsteady surface pressure fluctuations of microphone 18 for all porous leading edges, located at $x/c = 0.92$ (near to the trailing edge). The results of the porous cases demonstrate an increased energy level across the spectra compared to the results of the solid case. At the location of microphone 18, the highest energy level is demonstrated by the results of case P4, which has the most porous-occupied volume. The results of leading edge P4 also demonstrate the most significant increase of high frequency far-field noise compared to the results of the solid case. Between the frequencies of 100 Hz$< f <$ 400 Hz the results of case P4 are 10 dB/Hz in excess of the results of the solid case. However, the increased energy levels are not observed at high frequency. Interestingly, the increased energy levels are observed at low frequency where there is a reduction in the far-field noise.

The coherence between the surface pressure fluctuations in both the spanwise and streamwise direction are presented to gain an understanding of how the porous leading edge effects the development of coherent structures after the porous leading edge, over the surface of the airfoil. The magnitude-squared spanwise coherence is calcuated as,

$$\gamma^2_{p_{i'}p_{j'}}(f,\Delta z) = \frac{|\phi_{p_{i'}p_{j'}}(f)|^2}{|\phi_{p_{i'}p_{j'}}(f)||\phi_{p_{i'}p_{j'}}(f)|}, \tag{5}$$

where $\gamma^2_{p_{i'}p_{j'}}(f,\Delta z)$ represents the spanwise coherence calculated between two microphones separated by the spanwise distance Δz and locations z_i and z_j, and $\phi_{p_{i'}p_{j'}}$ is the cross power spectral density between the respective microphones. Figure 11 shows the spanwise coherence of the pressure fluctuations measured by five microphones with separations between 5.3 mm$< z <$ 25.3mm, at a streamwise location of $x/c = 0.25$ for the solid case and four porous cases at an angle of attack of $\alpha = 0°$. Figure 11a demonstrates the value of coherence peaks at 320 Hz for the closest separation of $z = 5.3$ mm, and reduces as the separation increases to $z = 25.3$ mm. The coherence value of each separation follows the same overall trend for the presented frequencies (200 Hz$< f <$ 6000 Hz), where coherence between the surface pressure fluctuation at multiple separations is only observed below $f < 700$ Hz. Above $f > 700$ Hz, there is no observed coherence between the surface pressure fluctuations in the solid case for all separations. For the porous leading edges, Figs. 11b to 11d, the coherence results exhibit similar behaviour, where coherence is observed below $f < 1000$

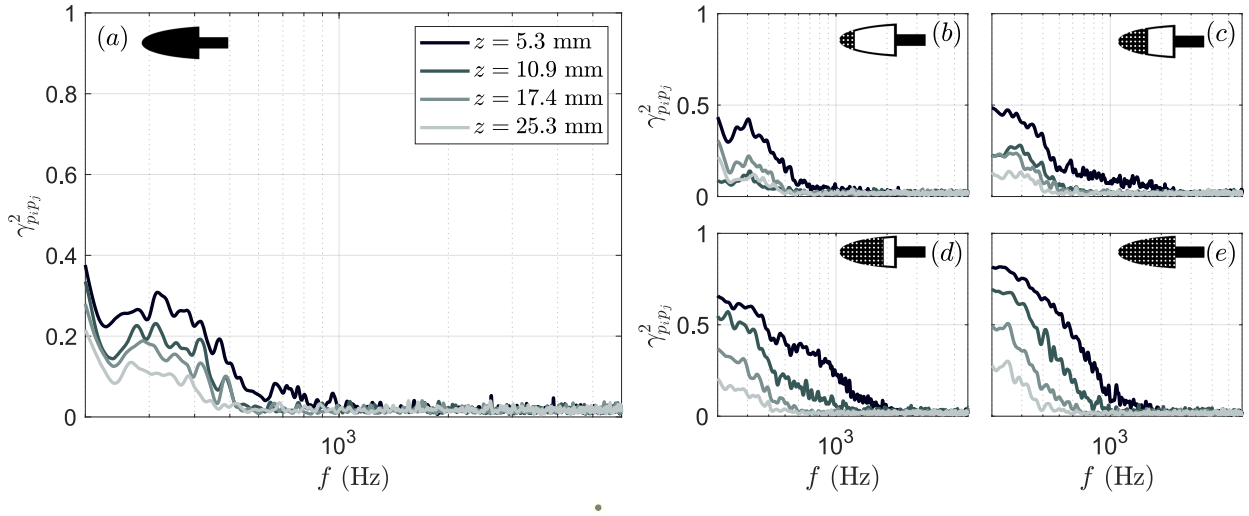

Fig. 11 Spanwise coherence of surface pressure fluctuations between spanwise microphones at chordwise locations $x/c = 0.25$ for the solid baseline compared to the porous leading edges at a free stream velocity of $U_\infty = 20$ m/s.

Hz, although as the percentage of chord which is occupied by the porous structure increases (P1 to P4), the level of coherence increases to a value of $\gamma^2_{p_i p_j} = 0.8$, for P4 with a separation of $z = 5.3$ mm. Generally, as the percentage of chord which is occupied by the porous structure increases, the level of coherence increases, in both magnitude and the frequency range in which coherence is observed.

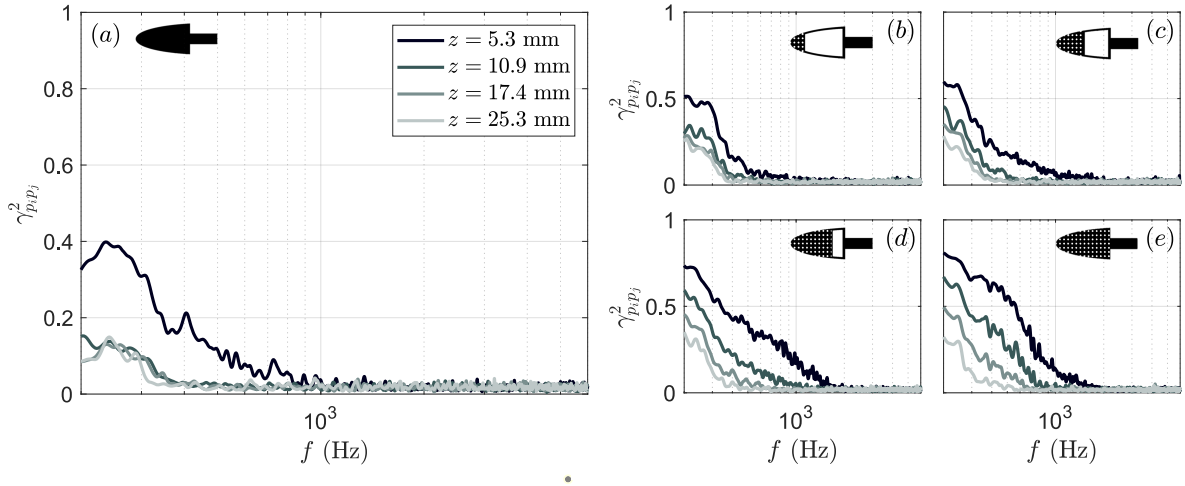

Fig. 12 Spanwise coherence of surface pressure fluctuations between spanwise microphones at chordwise locations $x/c = 0.36$ for the solid baseline compared to the porous leading edges at a free stream velocity of $U_\infty = 20$ m/s.

Figure 12 shows the spanwise coherence of the pressure fluctuation measured by five microphones with separations between 5.3 mm$< z <$ 25.3mm, at a streamwise location of $x/c = 0.36$ for the solid case and four porous cases at an angle of attack of $\alpha = 0°$. Figure 12 aids in identifying how the results of coherence develops downstream of the leading edge along the body of the airfoil for the solid leading edge and each porous case from $x/c = 0.25$ (Fig. 11) to $x/c = 0.36$ (Fig. 12). Considering Fig. 12 as a whole, the overall trend is similar to that of coherence results at $x/c = 0.25$. However, for the solid case (Fig. 12a) there is a distinct change in the behaviour of the coherence between the surface pressure fluctuations. For the results of separation distance $z = 5.3$ mm, the peak location has dropped to

f = 220 Hz and the value of coherence has increased. The results of the coherence for the larger separations in the solid case collapse on to one another an exhibit similar behaviour of lower coherence. For all porous cases at this chordwise location (x/c = 0.36), the level of coherence for all separations remains approximately consistent between the two streamwise locations of spanwise coherence.

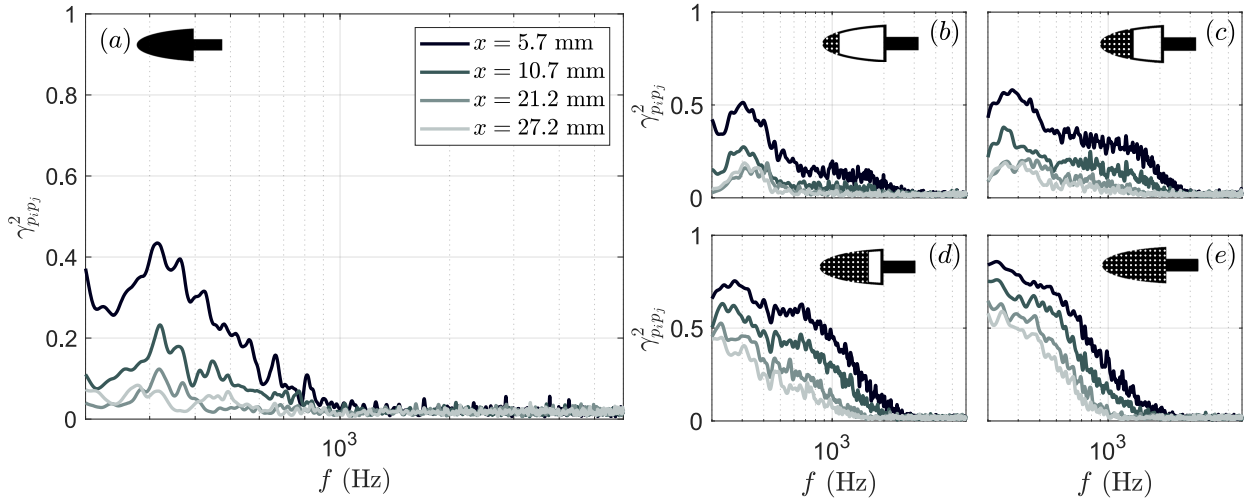

Fig. 13 Streamwise coherence of surface pressure fluctuations between multiple streamwise microphones and the streamwise microphone located at x/c = 0.25 for the solid baseline compared to the porous leading edges at U_∞ = 20 m/s.

The streamwise coherence is considered to evaluate the downstream coherence of the surface pressure fluctuations of the porous leading edges and how they compare to the solid case. The magnitude-squared streamwise coherence is calculated as,

$$\gamma^2_{p_{i'}p_{j'}}(f, \Delta x) = \frac{|\phi_{p_{i'}p_{j'}}(f)|^2}{|\phi_{p_{i'}p_{j'}}(f)||\phi_{p_{i'}p_{j'}}(f)|}, \tag{6}$$

where $\gamma^2_{p_{i'}p_{j'}}(f, \Delta x)$ represents the spanwise coherence calculated between two microphones separated by the streamwise distance Δx and locations x_i and x_j, and $\phi_{p_{i'}p_{j'}}$ is the cross power spectral density between the respective microphones. Figure 13 shows the streamwise coherence of the pressure fluctuation measured by five microphones along the surface of the airfoil at various chordwise positions. The streamwise coherence is considered between the microphone located at x/c = 0.25, and the downstream separations of x = 5.7 mm, x = 10.7 mm, x = 21.2 mm and x = 27.2 mm. The streamwise coherence of the surface pressure fluctuation (Fig. 13) is comparable to the spanwise coherence at the same chordwise position (Fig. 11). The highest level of coherence is observed for the closest separation of x = 5.7 mm and peaks at f = 320 Hz. In general, as the percentage-chord that is porous-occupied increases the level of coherence increases, across a range of frequencies up to 2000 Hz. The porous cases P1, P2 and P3 all exhibit a initial hump between 200 Hz< f < 400 Hz, which is comparable to the solid case. However, in the case of P4, a strong coherence is observed between 100 Hz< f < 500 Hz, which decays up to f = 2000 Hz. In contrast to the solid case, the results of the porous cases appear to have an increased coherence at higher frequencies between 700 Hz< f < 2000 Hz, where no coherence is observed in the solid case.

IV. Conclusion

Turbulence interaction noise between a turbulent inflow and an airfoil with various porous leading edges has been studied. The presented work employs an instrumented NACA0012 airfoil with an interchangeable leading edge, that was replaced with various porous leading edges of the same structure with varying chordwise amounts of porous-occupied volumes. It has been shown that the porous leading edge has little effect to the downstream value of pressure coefficient and the root-mean-square of the pressure coefficient. However, it is not possible to ascertain the effect of the porous structure on the suction peak at the leading edge of the airfoil due to limitations of instrumenting a porous leading edge. The far field noise analysis shows that systematically increasing the percentage chord of the porous-occupied volume at

the leading edge in turn reduces the leading edge noise at low frequency, but incurs a greater penalty at high frequency. Surface pressure analysis shows that increasing the porous-occupied volume at the leading edge increases the energy in the power spectral density of the pressure fluctuations at low frequency compared to the solid case, but no increase at higher frequencies compared to the solid case. Lastly, the coherence analysis of the surface pressure fluctuation in both the spanwise and streamwise direction showed that increasing the porous-occupied volume at the leading edge greatly increases the coherence between the pressure fluctuation of microphones at various separations across the airfoil in the spanwise direction and the streamwise direction.

Acknowledgments

The authors would like to acknowledge the financial support of Embraer S.A. and EPSRC.

References

[1] Paterson, R., and Amiet, R., "Acoustic radiation and surface pressure characteristics of an airfoil due to incident turbulence," Proceedings of the 3rd Aeroacoustics Conference, Palo Alto, CA, AIAA-76-571, 1976.

[2] Amiet, R., "Acoustic radiation from an airfoil in a turbulent stream," *Journal of Sound and Vibration*, Vol. 41, No. 4, 1975, pp. 407 – 420. https://doi.org/https://doi.org/10.1016/S0022-460X(75)80105-2.

[3] Moreau, S., and Roger, M., "Effect of Angle of Attack and Airfoil Shape on Turbulence-Interaction Noise," 11th AIAA/CEAS Aeroacoustics Conference, Monterey, CA, AIAA-2005-2973, 2005.

[4] Devenport, W. J., Staubs, J. K., and Glegg, S. A., "Sound radiation from real airfoils in turbulence," *Journal of Sound and Vibration*, Vol. 329, No. 17, 2010, pp. 3470 – 3483. https://doi.org/https://doi.org/10.1016/j.jsv.2010.02.022.

[5] Celik, A., Bowen, L., and Azarpeyvand, M., "Unsteady aerodynamic response of a NACA0012 in smooth and turbulent flows," AIAA AVIATION 2020 FORUM, AIAA-2020-2600, 2020.

[6] Hutcheson, F. V., Brooks, T. F., and Stead, D. J., "Measurement of the Noise Resulting from the Interaction of Turbulence with a Lifting Surface," *International Journal of Aeroacoustics*, Vol. 11, No. 5-6, 2012, pp. 675–700. https://doi.org/10.1260/1475-472X.11.5-6.675.

[7] Gill, J., Zhang, X., and Joseph, P., "Symmetric airfoil geometry effects on leading edge noise," *The Journal of the Acoustical Society of America*, Vol. 134, No. 4, 2013, pp. 2669–2680. https://doi.org/10.1121/1.4818769.

[8] Gill, J. R., Zhang, X., and Joseph, P., "Effects of Real Airfoil Geometry on Leading Edge Gust Interaction Noise," 19th AIAA/CEAS Aeroacoustics Conference, Berlin, Germany AIAA-2013-2203, 2013. https://doi.org/10.2514/6.2013-2203.

[9] Gershfeld, J., "Leading edge noise from thick foils in turbulent flows," *The Journal of the Acoustical Society of America*, Vol. 116, No. 3, 2004, pp. 1416–1426. https://doi.org/10.1121/1.1780575.

[10] Szoke, M., and Azarpeyvand, M., "Active Flow Control Methods for the Reduction of Trailing Edge Noise," Proceedings of the 23rd AIAA/CEAS Aeroacoustics Conference, Denver, CO, AIAA 2017-3004.

[11] Szőke, M., Fiscaletti, D., and Azarpeyvand, M., "Effect of inclined transverse jets on trailing-edge noise generation," *Physics of Fluids*, Vol. 30, No. 8, 2018, p. 085110.

[12] Showkat Ali, S. A., Azarpeyvand, M., and Ilário da Silva, C. R., "Trailing-edge flow and noise control using porous treatments," *Journal of Fluid Mechanics*, Vol. 850, 2018, pp. 83–119. https://doi.org/10.1017/jfm.2018.430.

[13] Showkat Ali, S. A., Azarpeyvand, M., Szőke, M., and Ilário da Silva, C. R., "Boundary layer flow interaction with a permeable wall," *Physics of Fluids*, Vol. 30, No. 8, 2018, p. 085111. https://doi.org/10.1063/1.5043276.

[14] Showkat Ali, S. A., Azarpeyvand, M., and da Silva], C. R. I., "Trailing edge bluntness noise reduction using porous treatments," *Journal of Sound and Vibration*, Vol. 474, 2020, p. 115257. https://doi.org/https://doi.org/10.1016/j.jsv.2020.115257.

[15] Liu, X., Jawahar, H. K., Azarpeyvand, M., and Theunissen, R., "Aerodynamic Performance and Wake Development of Airfoils with Serrated Trailing-Edges," *AIAA Journal*, Vol. 55, No. 11, 2017, pp. 3669–3680.

[16] Mayer, Y. D., Lyu, B., Jawahar, H. K., and Azarpeyvand, M., "A semi-analytical noise prediction model for airfoils with serrated trailing edges," *Renewable Energy*, Vol. 143, 2019, pp. 679 – 691. https://doi.org/https://doi.org/10.1016/j.renene.2019.04.132.

[17] Jawahar], H. K., Ai, Q., and Azarpeyvand, M., "Experimental and numerical investigation of aerodynamic performance for airfoils with morphed trailing edges," *Renewable Energy*, Vol. 127, 2018, pp. 355 – 367. https://doi.org/https://doi.org/10.1016/j.renene.2018.04.066.

[18] Celik, A., Mayer, Y., and Azarpeyvand, M., "An Experimental Aeroacoustic Study on Serrated Trailing-Edge Geometries and Flow Misalignment Effects," AIAA AVIATION 2020 FORUM, AIAA-2020-2518, 2020.

[19] Lyu, B., Azarpeyvand, M., and Sinayoko, S., "Noise Prediction for Serrated Leading-edges," 22nd AIAA/CEAS Aeroacoustics Conference, Lyon, France, AIAA-2016-2740, 2016.

[20] Lyu, B., and Azarpeyvand, M., "On the noise prediction for serrated leading edges," *Journal of Fluid Mechanics*, Vol. 826, 2017, p. 205–234. https://doi.org/10.1017/jfm.2017.429.

[21] Kim, J., Haeri, S., and Joseph, P., "On the reduction of aerofoil-turbulence interaction noise associated with wavy leading edges," *Journal of Fluid Mechanics*, Vol. 792, 2016, pp. 526–552. Data files are made available from http://dx.doi.org/10.5258/SOTON/397245 as required by EPSRC Research Data Policy.

[22] Narayanan, S., Chaitanya, P., Haeri, S., Joseph, P., Kim, J. W., and Polacsek, C., "Airfoil noise reductions through leading edge serrations," *Physics of Fluids*, Vol. 27, No. 2, 2015, p. 025109. https://doi.org/10.1063/1.4907798.

[23] Chaitanya, P., Joseph, P., Narayanan, S., Vanderwel, C., Turner, J., Kim, J. W., and Ganapathisubramani, B., "Performance and mechanism of sinusoidal leading edge serrations for the reduction of turbulenceaerofoil interaction noise," *Journal of Fluid Mechanics*, Vol. 818, 2017, pp. 435–464. https://doi.org/10.1017/jfm.2017.141.

[24] Roger, M., Schram, C., and Santana, L. D., "Reduction of Airfoil Turbulence-Impingement Noise by Means of Leading-Edge Serrations and/or Porous Material," 19th AIAA/CEAS Aeroacoustics Conference, Berlin, Germany, AIAA-2013-2108, 2013.

[25] Roger, M., and Moreau, S., "Airfoil Turbulence-Impingement Noise Reduction by Porosity or Wavy Leading-Edge Cut : Experimental Investigations," 2016.

[26] Geyer, T., Sarradj, E., Giesler, J., and Hobracht, M., "Experimental assessment of the noise generated at the leading edge of porous airfoils using microphone array techniques," 17th AIAA/CEAS Aeroacoustics Conference (32nd AIAA Aeroacoustics Conference), Portland, OR, AIAA-2011-2713, 2011.

[27] Geyer, T., Sarradj, E., and Giesler, J., "Application of a Beamforming Technique to the Measurement of Airfoil Leading Edge Noise," *Advances in Acoustics and Vibration*, Vol. 2012, 2012, pp. 1–16. https://doi.org/10.1155/2012/905461.

[28] Sarradj, E., and Geyer, T., "Noise Generation by Porous Airfoils," 13th AIAA/CEAS Aeroacoustics Conference (28th AIAA Aeroacoustics Conference), AIAA-2007-3719, 2007.

[29] Geyer, T. F., Lucius, A., Schrödter, M., Schneider, M., and Sarradj, E., "Reduction of Turbulence Interaction Noise Through Airfoils With Perforated Leading Edges," *Acta Acustica united with Acustica*, Vol. 105, No. 1, 2019, pp. 109–122. https://doi.org/doi:10.3813/AAA.919292.

[30] Roger, M., Schram, C., and Santana, L. D., "Reduction of Airfoil Turbulence-Impingement Noise by Means of Leading-Edge Serrations and/or Porous Material," 19th AIAA/CEAS Aeroacoustics Conference, Berlin, Germany AIAA-2013-2108, 2013.

[31] Carpio, A. R., Avallone, F., and Ragni, D., "On the Role of the Flow Permeability of Metal Foams on Trailing Edge Noise Reduction," 2018 AIAA/CEAS Aeroacoustics Conference, Atlanta, GA, AIAA-2018-2964, 2018.

[32] Sinnige, T., Corte, B. D., De Vries, R., Avallone, F., Merino-Martínez, R., Ragni, D., Eitelberg, G., and Veldhuis, L. L. M., "Alleviation of Propeller-Slipstream-Induced Unsteady Pylon Loading by a Flow-Permeable Leading Edge," *Journal of Aircraft*, Vol. 56, No. 3, 2019, pp. 1214–1230. https://doi.org/10.2514/1.C035250.

[33] Geyer, T. F., "Measurement of the turbulence interaction noise generated by flat plates with perforated leading edges," AIAA AVIATION 2020 FORUM, AIAA-2020-2576, 2020.

[34] Bampanis, G., and Roger, M., "On the Turbulence-Impingement Noise of a NACA-12 Airfoil with Porous Inclusions," AIAA AVIATION 2020 FORUM, AIAA-2020-2577, 2020.

[35] Zamponi, R., de Wyer, N. V., and Schram, C. F., "Experimental Investigation of Airfoil Turbulence-Impingement Noise Reduction Using Porous Treatment," 25th AIAA/CEAS Aeroacoustics Conference, Delft, Netherlands, AIAA-2019-2649, 2019.

[36] Mayer, Y. D., Jawahar, H. K., Szőke, M., Ali, S. A. S., and Azarpeyvand, M., "Design and performance of an aeroacoustic wind tunnel facility at the University of Bristol," *Applied Acoustics*, Vol. 155, 2019, pp. 358 – 370. https://doi.org/https://doi.org/10.1016/j.apacoust.2019.06.005.

[37] Mayer, Y., Zang, B., and Azarpeyvand, M., "Near-field aeroacoustic characteristics of a stalled NACA 0012 aerofoil," *Proceedings of the 23rd International Congress on Acoustics, integrating 4th EAA Euroregio 2019*, edited by M. Ochmann, DEGA e.V., 2019, pp. 5421–5428.

[38] Bowen, L., Celik, A., Azarpeyvand, M., and da Silva, C. R. I., "Design and Analysis of Turbulence Grids for Aeroacoustic Measurements," AIAA AVIATION 2020 FORUM, AIAA-2020-2525, 2020.

[39] Schwarz, H. A., *Gesammelte mathematische abhandlungen*, Vol. 260, American Mathematical Soc., 1972.

[40] Neovius, E. R., "Bestimmung zweier speciellen periodischen Minimalflächen, auf welchen unendlich viele gerade Linien und unendlich viele ebene geodätische Linien liegen," 1883.

[41] Bowen, L., Celik, A., Azarpeyvand, M., and da Silva, C. R. I., "On the use of Tailored Permeable Surfaces for Turbulence Interaction Noise Control," AIAA AVIATION 2020 FORUM, AIAA-2020-2530, 2020.